Quantitative Assessment of Burner Flame Stability through Digital Image Processing

Weicheng Xu, Yong Yan, *Fellow, IEEE*, Gang Lu, *Senior Member, IEEE*, and Xiaojing Bai

***Abstract*—Flame stability is a well-known problem in the power industry where low quality fuel is fired and combustion conditions change rapidly. Unstable flames often lead to lower combustion efficiency, higher pollutant emissions, and other operational problems. Although there are many methods available for flame monitoring and characterisation, very few are suitable for flame stability monitoring. This paper presents a method for the quantification of flame stability by introducing a term called flame stability index through digital imaging and image processing. This index combines variability of several characteristic parameters of a flame. The stability index of a premixed methane-air flame for the equivalence ratio ranging from 0.36 to 2.17 and methane-biomass flames for ten biomass fuels is measured on a laboratory-scale combustion test rig. For purpose of comparison the flame stability is also measured in terms of oscillation frequency and with two earlier methods. Results show that correlation coefficient between the stability index and the oscillation frequency is greater than 0.89, indicating that the stability index characterises the flame stability. In addition, the stability index is more sensitive to the variation in flame stability than the oscillation frequency and its quantification requires a shorter data length. The proposed method outperforms the other two earlier methods, although the latter also combines characteristic parameters of the flame through summation or mean-square calculation. Unlike the earlier methods, the stability index determined using the proposed methods is capable of quantifying flame stability regardless of combustion conditions.**

***Index Terms*—Flame stability; Flame monitoring; Digital imaging; Image processing.**

I. Introduction

MONITORING and characterising the stability of various fuels fired flames in furnaces has become more important than ever due to the recent trend of using a wide range of biomass, biofuels, and low-ranking coals [1]. An unstable flame can cause many combustion problems, such as furnace vibration, low combustion efficiency, high NOx emissions, and even flameouts [2]. In addition, the operation of power plants must be flexible in order to accommodate the intermittency of fluctuating demand by the users and increasing levels of renewable sources such as wind farms and solar stations. The combustion process should be continuously optimized for a range of fuels under variable load demand and flexible operation conditions. It is therefore important to develop a reliable and effective method for the online continuous quantification of flame stability.

Flame stability is a broad concept largely relating to burner structure [3], air-to-fuel ratio [3], ignitability of the fuel [4], and velocity of the air-fuel mixture [5]. Significant research has been conducted computationally and experimentally to investigate the mechanism and characteristics of flame stability through computational modelling, such as Euler simulation [6] and large eddy simulation [7], and diagnostic observations through the use of laser-induced fluorescence [8], infrared absorption [9] and digital imaging [10]. Digital imaging has been identified as one of the most effective approaches to advanced flame monitoring in terms of system functionality, operability, and cost-effectiveness [11]. With the advances in imaging sensors and image processing algorithms, online continuous quantitation of flame stability has become possible. The methods currently available for assessing flame stability through digital imaging are based on the determination of flame characteristic parameters such as oscillation frequency [12], characteristics of the root region [13], colour information [14], and other parameters of flame images [15].

Flame oscillation frequency is a common indicator that has been used to evaluate flame stability for some years. Huang et al. [14] studied the relationship between the oscillation frequency of a gaseous flame and the variations in the radiation intensity of the flame images from a common visible-range camera. Chimenti et al. [16] used a near-infrared camera to record the images of a premixed hydrogen-air jet flame and characterised flame stability in terms of oscillation frequency of the geometric features of the flame. Lu et al. [17] determined the stability of a coal-biomass flame by determining the oscillation frequency of the radiation intensity of the flame from a video stream. De Giorgi et al. [18] used a common visible-range camera and a near-infrared camera to capture the flame zones, respectively. The flame stability was characterised through the analysis of the frequency and wavelet energy of the pixel intensities in flame images. However, there are limitations in these methods. It has been known for a long time that the

Manuscript received Month xx, 20xx; revised Month xx, 20xx; accepted Month xx, 20xx. This work was funded by the National Natural Science Foundation of China under Grant No. 51827808. The Associate Editor coordinating the review process was xx. (*Corresponding author: Yong Yan*)

Weicheng Xu and Xiaojing Bai are with the School of Control and Computer Engineering, North China Electric Power University, Beijing 102206, China (e-mail: xwc2357@gmail.com; baixiaojing1987@163.com).

Yong Yan and Gang Lu are with the School of Engineering, University of Kent, Canterbury, Kent CT2 7NT, UK (e-mail: y.yan@kent.ac.uk; g.lu@kent.ac.uk).

flame oscillation frequency due to natural convection on traditional laboratory burners lies typically between 7 and 15 Hz for many fuels fired in air at a pressure of 1 atm [18]. The higher the oscillation frequency, the more stable the burner flame [14]. This general rule is usually applied to assessing the flame stability by comparing oscillation frequencies under the same combustion conditions [14]. However, as the combustion conditions change significantly, the same oscillation frequency may represent different flame stabilities. Many factors such as fuel type [19], chamber pressure [20] and burner configurations [21] influence the oscillation frequency of a burner flame. In summary, the oscillation frequency is not a reliable indicator for flame stability in many cases, though it is useful under some well-defined combustion conditions.

The root region of a flame is the primary reaction zone of a combustion process in terms of energy conversion and emission formation. The flame stability is thus often evaluated by characterising the root region of the flame. Smart et al. [22] analysed the oscillation frequency of the radiation intensity of the root region of an oxy-fuel flame on a 0.5 MWth coal fired combustion test rig. The oscillation frequency of the oxy-fuel flame was observed in relation to the recycle ratio, total flow, and total O_2 for pulverised coal. Pan et al. [13] assessed the stability of a premixed methane-air flame by assessing whether the flame root is attached to the burner outlet or not. The flame stability was quantified by analysing the fluctuation of the brightness of the root region. Samantaray et al. [23] analysed a natural gas flame and a coal-biomass flame in a 500 kW pulverised fuel fired pilot swirl combustor through image processing. The flame stability was characterised in terms of statistical and spectral features of the root region. However, these studies have focused on the reflection of the flame stability on the root region, but have ignored the information in other parts of the flame. In other words, the flame stability information from the root region does not reflect the full extent of the flame stability.

Apart from the oscillation frequency of the whole flame and the characteristics of the root region, some efforts have also been made to assess the flame stability through statistical analysis of the physical parameters of the flame such as its colour and edges. Najarnikoo et al. [24] investigated the colour characteristics of the flames in a cylindrical perforated burner and analysed the variations of the flame stability with the equivalence ratio. The flame stability is characterised by the intersection of the intensity components of red and blue channels in the flame images. Sun et al. [25,26] quantified the stability of a heavy-oil fired flame by combining the colour information of the flame in the HSI (Hue, Saturation, and Intensity) space [25] and characteristic parameters such as length, luminous region and brightness [26]. The impact of the swirl vanes on the flame stability quantified using the approaches in [25,26] was investigated. Matthes et al. [15] used the variation rate of the edges of a pulverised coal flame to characterise the flame stability. It must be pointed out that the flame stability quantified in terms of geometric and luminous characteristics of the flame depends significantly on the installation position of the camera on the furnace and the quality of the flame images.

The existing methods for quantifying flame stability concentrate mainly on the usage of different characteristic parameters in an isolated manner. Although they can work under some specific conditions, they do not work well in other conditions. This paper presents a comprehensive method for the continuous and quantitative measurement of flame stability by combining the variability of all the effective characteristic parameters derived from flame images. A data processing method is proposed concomitantly to acquire the effective parameters and their variability which are closely associated with flame stability. The acquisition of the effective parameters and their combination for flame stability monitoring have never been reported previously.

II. Methodology

A. Overall strategy

Flame stability is generally reflected in the variability of a range of characteristic parameters of the flame. The overall strategy for the measurement of flame stability is illustrated in Fig. 1. There are two main stages in the strategy, i.e., the determination of flame parameters and quantification of flame stability. In the first stage, all flame parameters, including geometric, luminous, and thermodynamic parameters, be identified and determined from the flame images. In the second stage, the variability of the flame parameters are quantified by determining their statistical characteristics. The parameters that contain useful flame stability information are regarded as *effective* parameters. The effective parameters are separated into normal and abnormal categories according to a variability scale. Then, the flame stability is determined through statistical analysis of the normal and abnormal variability of the parameters.

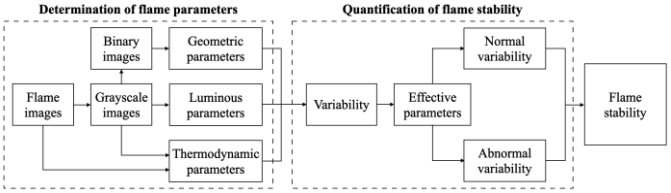

Fig. 1. Overall strategy for the quantification of flame stability.

B. Determination of flame parameters

It is a prerequisite to define and determine all the possible flame parameters before quantifying the flame stability. The digital images of a flame are normally captured using a digital camera. Each flame image is normally a two-dimensional projection of a three-dimensional flame on the imaging element of the camera. A range of physical parameters of the flame, which provide instantaneous information on the combustion process, can be determined by processing the flame images using appropriate digital image processing algorithms. The parameters characterising a flame vary, depending upon various factors such as the type of the furnace, physical location of the viewing port, field-of-view of the imaging system etc. In the present study, the flame parameters are classified into three categories, i.e., geometric, luminous, and thermodynamic

Table I. Flame parameters

Category	Name	Symbol	Unit
Geometric parameters	Ignition point	L_{ip}	mm
	Area of root region	A_{root}	%
	Spreading-angle	α_s	°
	Length	L	mm
	Area	A	%
Luminous parameters	Brightness	B_f	%
	Nonuniformity	NU_f	%
Thermodynamic parameters	Max temperature	T_{max}	°C
	Min temperature	T_{min}	°C
	Mean temperature	T_{mean}	°C
	Oscillation frequency	F	Hz

parameters, as listed in Table I. Since many of the parameters were defined elsewhere [27, 28], only a brief introduction to them is given here for the convenience of the reader. It is worth noting that, since the spectra of a flame extend over a wide range of wavelengths [24], the definitions of the parameters may vary if the flame images are captured in different bands of the spectra. The parameters presented here are specifically defined for flame images in the visible range, which are more readily available from common digital cameras than those in other spectral bands such as hyperspectral and infrared cameras. In principle, however, the methodology presented in this paper is applicable to flame images in other spectral bands.

1) *Geometric Parameters:*

Geometric parameters represent the fundamental geometric characteristics of the flame in its images. The definitions of the geometrical parameters are illustrated in Fig. 2. Note that, in view of the fact that burners in most practical furnaces are horizontally arranged, a typical horizontal flame is illustrated here. The definition and determination of the flame parameters in other orientations are similar to those of a horizontal flame.

(*a*) *Ignition point* (L_{ip}) represents the absolute distance between the burner outlet and illuminating points $I_p(i_{ip}, j_{ip})$ where the fuel is ignited in the flame front. L_{ip} is the minimum distance from the burner outlet to the nearest illuminating point, i.e.,

$$L_{ip} = k_{IMG} \min\left(i_{ip}\right) \tag{1}$$

where i_{ip} is the location of the illuminating point at the flame front. k_{IMG} is the scale factor which converts the physical dimension from number of pixels to meters. A stable flame has a steady flame front at which the heat lost and heat release of the fuel are well balanced. The flame front is a three-dimensional dynamic surface comprising all the ignition points. The ignition points recorded in a flame image are the two-dimensional projection of the flame front and are used here for evaluating the stable state of the flame front. The ignition point depends on the burner structure and fuel type and is only available for a detached flame. For an attached flame where the fuel is ignited inside the burner outlet, the ignition point is not visible [29].

(*b*) *Area of root region* (A_{root}) is defined as the area of the illuminating region in the root of the flame normalised to a rectangular bounding box, which is located immediately adjacent to the burner outlet, as shown in Fig. 2. Although the

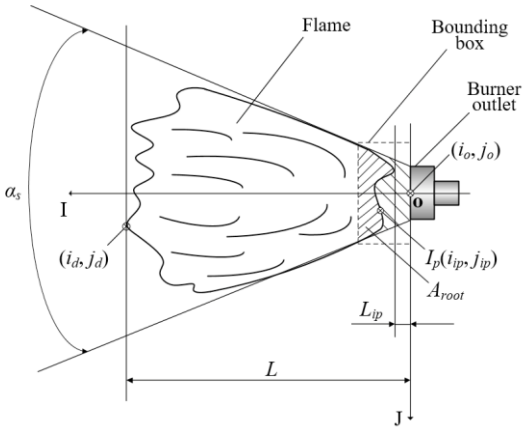

Fig. 2. The definitions of the geometrical parameters.

area of root region of a flame has been used for evaluating the flame stability in [13], it is re-defined here for a wider applicability. A_{root} is determined from the following equation:

$$A_{root} = \frac{1}{A_{bb}} \sum_{i \in R_{root}} \sum_{j \in R_{root}} B_{root}(i, j) \times 100\% \tag{2}$$

where A_{bb} is the total number of pixels in the bounding box. The lengths of two horizonral lines of the box (Fig. 2) are equal to the diameter of the burner outlet. The vertical line parallel to the burner outlet is twice the diameter of the burner outlet. It should be noted that the size of the bounding box must be adjusted for special burners and fuels in order to encompass the flame front. R_{root} represents the luminous region in the box; $B_{root}(i, j)$ equals 1 at (i, j) in R_{root}. The root region is the primary reaction zone of a combustion process. In the root region, the heat release in the reaction between the fuel and oxidizer is related to the flame stability [30]. Non-uniformly distributed heat release may lead to an unstable flame which is characterised by changes in the root region characteristics, such as the brightness and area of the root region. If the flame is extremely unstable, the root detaches from the burner outlet and its area varies substantially [31].

(*c*) *Spreading-angle* (α_s) is defined as the angle formed between the two straight lines scribing from the burner outlet to the outer edges of the flame, as shown in Fig. 2, i.e.,

$$\alpha_s = \frac{180}{\pi} \arctan\left(\left|\frac{k_2 - k_1}{1 + k_1 k_2}\right|\right) \tag{3}$$

where k_1 and k_2 are the gradients of the two straight lines, respectively. The two lines are commonly asymmetrical about the burner axis [32]. The variations in the spreading-angle are associated with the changes in the local reaction rate across the flame surface [33]. The spreading-angle is normally measurable in turbulent jet flames, but not in some cases where the fitted edges are in parallel or intersect at a point downstream of the flame.

(*d*) *Length* (*L*) represents the absolute distance between the burner outlet and the furthest illuminating point at the tip of the flame. This point, (i_d, j_d), is identified by searching the illuminating points in the flame image along the burner axis. The length of the flame is thus determined from

$$L = k_{IMG} i_d \tag{4}$$

The change in the length of a flame is related to the transient convective flow induced by the vortices and the transition of the stable state of the flame [34].

(*e*) *Area* (*A*) is a measure of the cross-sectional area of the luminous region with reference to the whole viewing field, i.e.,

$$A = \frac{1}{A_{image}} \sum_{i \in R_f} \sum_{j \in R_f} B(i, j) \times 100\% \tag{5}$$

where $B(i, j)$ is 1 at (i, j) in the luminous region (R_f) of the flame. A_{image} is the total number of pixels in the flame image. The variation in A is related to the heat release rate which reflect the stability of the flame [34].

2) *Luminous Parameters:*

All burner flames exhibit some form of optical radiative emissions due to the nature of combustion process. Luminous parameters of a flame represent its radiative heat transfer characteristics in the electromagnetic spectrum. Two luminous parameters, i.e., brightness and nonuniformity, are determined from the greyscale images and used for evaluating the luminous properties of the flame. The greyscale images are transformed from the original images, i.e., [35]

$$I = 0.30R + 0.59G + 0.11B \tag{6}$$

where R, G, and B are red, green, and blue components in RGB colour space, respectively. I is a weighted sum of the three individual components in the RGB colour space and represents the radiation intensity distribution of the flame.

(*a*) *Brightness* (B_f) is defined as the mean grey-level of the luminous region normalised to the maximum grey-level, i.e., 255 for an 8-bit digital image, i.e. [27],

$$B_f = \frac{1}{255} \sum_{i_G \in R_f} \sum_{j_G \in R_f} \frac{1}{A} G(i_G, j_G) \times 100\% \tag{7}$$

where $G(i_G, j_G)$ is the grey-level at (i_G, j_G) in the luminous region (R_f) of the flame (I). B_f ranges between 0 and 100%. A greater value of B_f means a brighter flame.

(*b*) *Nonuniformity* (NU_f) represents the relative deviation of the luminous intensities of the 'darker' and 'brighter' parts of the flame [27], i.e.,

$$NU_f = \frac{\sum_{k=\delta_f}^{255} n(k) \left| B(k) - B_f \right|}{N_p B_f} \times 100\% \tag{8}$$

where $n(k)$ is the number of pixels at the grey-level $B(k)$ (0-255). N_p is the total number of pixels within the luminous region. NU_f ranges from 0-100 % with 0 % meaning the flame is completely uniform in the luminous region.

3) *Thermodynamic Parameters:*

Thermodynamic parameters represent the external manifestation of the chemical reaction in a flame in terms of heat release and oscillatory nature of the combustion process. They include the temperature and oscillation frequency.

(*a*) *Temperature* (T) is one of the most important characteristics of the flame. The variation in the temperature distribution reflects the process of radiative heat transfer and is closely related to flame stability [36]. The flame temperature distribution can be determined from flame images through two-colour pyrometry [37]. In the two-colour method, 2-D temperature distribution of a flame, $T(i, j)$, is derived from the relationship between the flame intensities at two pre-defined wavelengths based on the Planck radiation law [38], i.e.,

$$T(i, j) = \frac{C_2 \left(\frac{1}{\lambda_2} - \frac{1}{\lambda_1} \right)}{\ln \frac{G[\lambda_1, (i, j)]}{G[\lambda_2, (i, j)]} + S + \ln \left(\frac{\lambda_1}{\lambda_2} \right)^5} \tag{9}$$

where C_2 is the second Planck's constant, (i, j) is the coordinate in the luminous region (R_f), $G[\lambda_1, (i, j)]$ and $G[\lambda_2, (i, j)]$ are the grey-levels of the flame images which are obtained at the two pre-defined wavelengths, λ_1 and λ_2, respectively, and S is the instrument factor, which is obtained through calibration of the imaging system [39]. In the case where RGB images are used, λ_1 and λ_2 are the peak wavelengths of the red and green channels of the flame images, respectively.

In order to characterise the flame temperature distribution, three temperatures, i.e. maximum temperature (T_{max}), minimum temperature (T_{min}), and mean temperature (T_{mean}) are defined as follows,

$$T_{max} = \max \{ T(i, j) \} \tag{10}$$

$$T_{min} = \min \{ T(i, j) \} \tag{11}$$

$$T_{mean} = \frac{1}{N_p} \sum_{i \in R_f} \sum_{j \in R_f} T(i, j) \tag{12}$$

It is worth noting that there are other techniques for flame temperature measurement such as radiation method [39]. Variants of the two-colour method, e.g., three-colour methods [40] are also available. Since the evaluation of flame stability is based on the variability of the flame parameters, the actual method used for flame temperature maurement is not critical in flame stability quantification.

(*b*) *Oscillation frequency* (F) is determined as the power-density weighted average frequency over the entire frequency range of the flame signal [28], i.e.,

$$F = \frac{\sum_{i=0}^{N_f} [P(f_i) f_i]}{\sum_{i=0}^{N_f} P(f_i)} \tag{13}$$

where f_i is the i^{th} frequency component in the frequency spectrum, $P(f_i)$ is the power density of the i^{th} frequency component, and N_f is the total number of frequency components. The flame signal here is obtained by processing the combined luminous intensity of all the individual pixels within the greylevel image of a flame (I) as a function of time.

Previous studies suggested that the low-frequency components of a flame signal originate from the geometrical fluctuations of the flame due to the aerodynamic or convective effect, whilst high-frequency components may be due to the energy transitions among intermediate radicals or variations in the energy emission rate of reacting species [28]. However,

flame stability cannot be represented by a single oscillation frequency as discussed in Section I. The variation in the oscillation frequency should be considered in the flame stability assessment instead of the oscillation frequency itself.

C. Quantification of flame stability

1) Existing methods and their limitations

There are established methods for evaluating flame stability through statistical analysis of flame parameters [25, 26]. One of the methods combines the colour and geometric information of the flame [25]. The flame information considered in the flame stability quantification includes hue (H), saturation (S), and intensity (I) of flame colour as well as the flame area. Their statistical characteristics were assigned as M_H, M_S, M_I, C_H, C_S, C_I, and A_I, M_H, M_S, where M and C denote the mean and contrast of the individual H, S, and I components, respectively, A_I is the flame area, which is derived from the I image and normalised to the size of the image. In this method the flame stability index is defined as

$$\delta = \prod_{i=1}^{7}\left(\frac{\phi(i)-\sigma(i)}{\phi(i)}\right)^{w_{mp}(i)} \tag{14}$$

where $\sigma(i)$ is the standard deviation of the i^{th} statistical characteristic and $\phi(i)$ represents the theoretical maximum of $\sigma(i)$, i=1-7. $w_{mp}(i)$ is the weighting index for the i^{th} statistical characteristic. In the reported study [25] $w_{mp}(i)$=2 was assigned for all the characteristics, suggesting that all the characteristics were taken as equally important, though different $w_{mp}(i)$ may be assigned in principle. For convenience of presentation, we regard this method as "multiplication method".

The other method extracts information from RGB flame images, including ignition points (maximum, minimum and mean), length, luminous region, brightness, and nonuniformity [26]. The flame stability index is defined as

$$\delta = \sqrt{\sum_{i=1}^{7}\left(\frac{w_{rs}(i)\sigma(i)}{\mu(i)}\times 100\%\right)^2} \tag{15}$$

where $\sigma(i)$ and $\mu(i)$ are the standard deviation and mean of the i^{th} flame parameter, respectively. $w_{rs}(i)$ is the weighting for the corresponding parameter and $\sum_{i=1}^{7} w_{rs}(i)^2 = 1$. In view of the logic used in combining the flame parameters, this method is regarded as "root-square method" in this paper.

The two existing methods have limitations. First, it is assumed in both methods that the weightings of the individual flame parameters are the same, but this assumption may not be valid in practice. A higher weighting should be given for the parameter which is more sensitive to the change in flame stability. Second, the flame parameters used in both cases may only evaluate the flame stability under specific, narrow range of combustion conditions, as reported in the references [25, 26]. Variations in combustion conditions may make the two methods ineffective. In consideration of these limitations of the existing methods, this paper proposes a new method in quantifying flame stability by assigning different weightings to the different flame parameters. The method is expected to perform well under a wider range of combustion conditions.

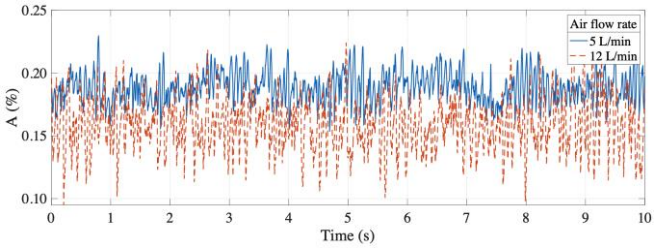

Fig. 3. Variations in the area of methane-air premixed flames at methane flow rate 1.00 L/min for air flow rates of 5 L/min and 12 L/min.

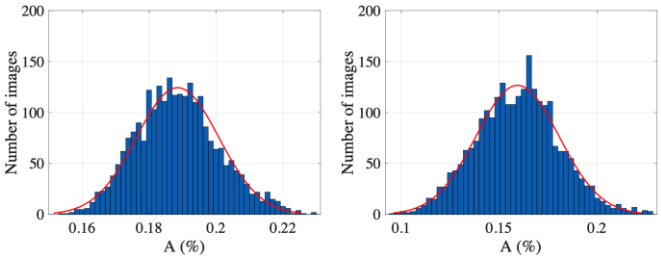

(a) 5 L/min (b) 12 L/min

Fig. 4. Area distributions at methane flow rate 1.00 L/min for air flow rates of 5 L/min and 12 L/min.

2) Variability of flame parameters

The variability characteristics of a parameter are reflected in its observed variations with time. Take flame area as an example, Fig. 3 shows the variations in the area (A) of methane-air premixed flames with time. The flame video was recorded using a colour CMOS camera on a laboratory-scale combustion test rig. The detailed information about the rig and the flame is described in Section III. It can be seen from Fig. 3 that the area varies around a mean value within a range under each condition due to the inherently dynamic nature of the flame. The dataset follows the normal distribution for each combustion condition (Fig. 4). The variability of the area varies clearly with the air flow rate for a given methane flow rate, reflecting different stable states of the flame. Such variability can be quantified by the dispersion of the parameters from the mean, i.e.,

$$\delta_x = \frac{\sigma_x}{\mu_x}\times 100\% \tag{16}$$

where σ_x and μ_x are the standard deviation and mean of the parameter x, respectively.

3) Effectiveness of flame parameters

The variability of some parameters may not contain useful information about the flame stability. In this case such parameters are considered ineffective. They should be identified and excluded in order to avoid their impact on quantifying the flame stability. This can be done based on the correlation analysis between the variability of the parameters (δ_x) and the oscillation frequency of the flame. The correlation coefficient (CC) is calculated as,

$$CC = \frac{\sum_{i=1}^{N_c}\left(\delta_{x(i)}-\overline{\delta_x}\right)\left(F_i-\overline{F}\right)}{\sqrt{\sum_{i=1}^{N_c}\left(\delta_{x(i)}-\overline{\delta_x}\right)^2\sum_{i=1}^{N_c}\left(F_i-\overline{F}\right)^2}} \tag{17}$$

where $\delta_{x(i)}$ and F_i are the variability of the parameter x and oscillation frequency in the i^{th} measurement, respectively, N_c is

the number of measurements in each measurement cycle, and $\overline{\delta}_x$ and $\overline{F}$ denote the mean values of $\delta_{x(i)}$ and F_i, respectively. A high correlation coefficient means that the variability of a parameter shares a similar trend with the oscillation frequency and thus contains useful information about the flame stability. This parameter is thus considered as an effective parameter. Otherwise, a parameter is regarded as ineffective. An appropriate threshold for the correlation coefficient has to be set to determine if a parameter is 'effective' or 'ineffecive', which is discussed in Section 4. Note that the correlation coefficient is only used to suggest whether the variability contains useful stability information. A higher correlation coefficient does not mean that more useful information is contained in the flame parameter.

4) *Normal and abnormal variability*

As described in Section II.*C*(2), the dataset of a flame parameter follows the normal distribution (Fig. 4). The values lying in the range between ± two standard deviations from the mean with 95% confidence limits are defined as usual values. Meanwhile, the values falling outside ± two standard deviations are defined as unusual values. The usual and unusual value are processed to obtain the normal and abnormal variability, respectively.

The normal variability is determined by the dispersion of the usual values from their mean, i.e.,

$$\delta_{x-nor} = \frac{\sigma_{x-nor}}{\mu_{x-nor}} \tag{18}$$

where $\delta_{x\text{-}nor}$ represents the degree of the variability of the parameter *x*, and $\sigma_{x\text{-}nor}$ and $\mu_{x\text{-}nor}$ are the standard deviation and mean of the usual values of the parameter *x*, respectively. The normal variability reflects the most common and basic characteristics of the flame. Thus, it is the basis for quantifying the flame stability.

The abnormal variability is represented by an instability coefficient and normal variability together, i.e.,

$$\delta_{x-abnor} = C_x \delta_{x-nor} \tag{19}$$

where C_x is the instability coefficient, which represents the variability of the unusual values of the parameter x and is defined as,

$$C_x = \frac{X_{x-upper} - X_{x-lower}}{\mu_{x-nor}} \tag{20}$$

where $X_{x\text{-}upper}$ and $X_{x\text{-}lower}$ are determined as follows,

$$X_{x-upper} = \mu_{x-upper} - 2\sigma_x \tag{21}$$

$$X_{x-lower} = \mu_{x-lower} + 2\sigma_x \tag{22}$$

where $\mu_{x\text{-}upper}$ and $\mu_{x\text{-}lower}$ are the mean values of the unusual values which are two standard deviations above and below the mean ($\mu_{x\text{-}nor}$), respectively, if the unusual values exist. $X_{x\text{-}upper}$ and $X_{x\text{-}lower}$ represent the extent to which the large and small unusual values deviate from the mean ($\mu_{x\text{-}nor}$), respectively. The abnormal variability of the flame in terms of characteristic parameters are a manifestation of flame stability. A higher instability coefficient should be applied to a parameter which exhibits larger unusual values as this parameter is more sensitive to the change in flame stability than the other effective parameters. A parameter is considered as the most important one in the flame stability evaluation if it has the most significant variability and highest instability coefficient. The most important parameter means that it reflects the flame stability best under specific combustion conditions.

5) *Flame stability index*

The stability of a flame is manifested in the variability of effective parameters. A term named flame stability index (δ) combines such information to quantify the flame stability and is defined as,

$$\delta = \left(\frac{1}{N_e} \sum_{i=1}^{N_e} (1 + C_{x(i)}) \delta_{x(i)} \right)^{(1+C_F)\delta_F} \tag{23}$$

where N_e is the number of effective parameters, $x(i)$ is the i^{th} effective parameter, $C_{x(i)}$ and $\delta_{x(i)}$ are the instability coefficient and normal variability of $x(i)$, respectively. C_F and δ_F are the instability coefficient and normal variability of the oscillation frequency, respectively.

The variability of effective parameters contain useful information about the flame stability. The integration of these parameters is to reflect flame stability comprehensively in a range of perspectives. The variability of the oscillation frequency serving as the exponent in equation (23) increases the sensitivity of the stability index to the change in the flame stability. An increased δ means that one or more parameters vary substantially, i.e., the flame is unstable. The closer the index to 0, the more stable the flame. Note that the flame stability index has no theoretical upper limit due to different limits that flame extinguishes under different combustion conditions.

Unlike the multiplication or root-square methods [25, 26], this proposed "weighted average" method can be used for flame stability determination under a wider range of combustion conditions. All possible flame parameters are extracted from flame images and those effective ones are combined to determine the flame stability. If combustion conditions change, the effectiveness of all the flame parameters are re-determined. Since only the effective parameters are combined, this method can achieve good flame stability results under any combustion conditions. The other advantage of this method over the two existing ones [25, 26] is the use of uneven parameter weighting, which is characterised by the instability coefficient, in the combination of effective parameters. Further details about the instability coefficient are given in Section 4.1.3. Moreover, oscillation frequency is also incorporated in the flame stability index, which is not considered in the existing methods [25, 26].

III. Test Conditions and Experimental Programmes

A. Combustion test rigs

To evaluate the effectiveness of the proposed method, a series of experiments were carried out on a laboratory-scale combustion test rig. As shown in Fig. 5, the test rig consists of an air compressor, a fuel tank, a flow rate controller, a biomass feeder, a burner and a combustion chamber. The flow rates of

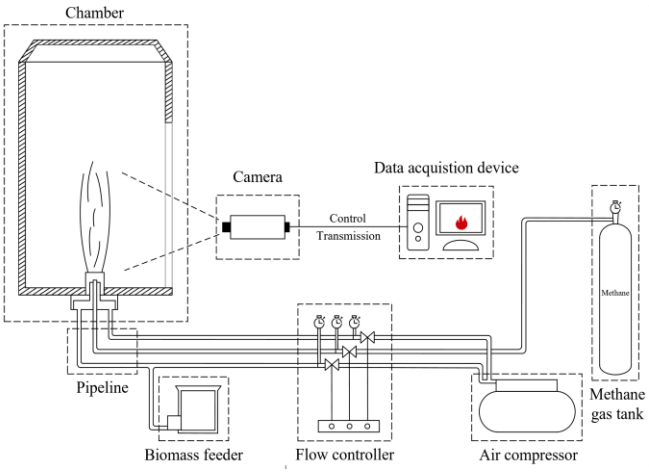

Fig. 5. Schematic diagram of the laboratory-scale combustion test rig.

air and methane are metered and controlled using the flow rate controller. The flame is ignited at the burner outlet in the combustion chamber. The diameter of the burner outlet is 2.4 cm. A mesh screen is mounted across the burner outlet to stabilise the flame. A CMOS camera with a resolution of 1280×1024 pixels was used to acquire flame images at a frame rate of 250 frames per second. The shutter speed was 1/250 second. The distance between the camera lens and centre of the burner outlet is 140 cm.

B. *Experimental programmes*

1) *Methane-air premixed flames*

Since methane is a good gaseous fuel with controllable flame stability, the methane flame is used as a reference in this study for the stability assessment of other fuels. Various equivalence ratios were created to vary the stability of the methane flame. The equivalence ratio Φ is recognised as one of the most important factors in relation to fuel conversion, pollutant emissions, and flame stability [11], which is defined as [41]:

$$\Phi = \frac{m_{\text{fuel}}/m_{\text{air}}}{(m_{\text{fuel}}/m_{\text{air}})_{\text{st}}} \tag{24}$$

where $m_{\text{fuel}}/m_{\text{air}}$ and $(m_{\text{fuel}}/m_{\text{air}})_{\text{st}}$ represent the actual and stoichiometric fuel-to-air ratios, respectively. The stoichiometric fuel-to-air ratio is the chemically correct fuel-to-air ratio required for complete combustion of the fuel [41]. Different premixed flames are created by adjusting air flow rates at a fixed fuel flow rate. In this study, the air flow rate was varied over the range of 4-14 L/min with an increment of 1 L/min for three fixed methane flow rates of 0.5 L/min, 0.75 L/min, and 1.00 L/min, respectively. The resulted equivalence ratio Φ ranges from 0.36 to 2.17.

2) *Biomass flames*

Biomass fired power generation can significantly increase the share of renewable energy sources and reduce CO_2 emissions. To investigate the effectiveness of the stability index in measuring the stability of biomass flames, a series of experiments was also conducted on the test rig (Fig. 5). Different kinds of biomass, i.e., peanut shell, willow, wheat straw, corncob, and their blends as shown in Table II, were injected into the pipeline feeding the burner using the biomass feeder at 2 Hz. The mixture of the biomass, methane and air was then fired at the burner. The flow rates of air and methane were set to 8.0 L/min and 0.5 L/min, respectively.

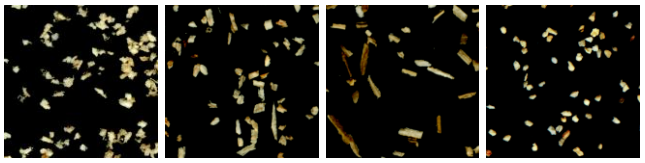

Fig. 6. Images of the biomass particles.

The proximate and ultimate analyses of the four biomass fuels are summarised in Table III. The volatile matters and fixed carbon are combustible components. As can be seen, among the four biomass fuels, the corncob and wheat straw are the most combustible and less combustible fuels, respectively. Fig. 6 shows the images of the biomass particles with their corresponding particle size and shape distributions summarized in Table IV. These results were obtained using a digital imaging-based particle size analyser (OMEC-LS-POP(9)) [42]. Table IV indicates that, among the four types of biomass fuels, peanut shell and wheat straw have the smallest and largest particle sizes, respectively. The wheat straw and corncob have the largest and smallest aspect ratios, respectively.

IV. RESULTS AND DISCUSSION

A. *Methane-air premixed flames*

1) *Effective flame parameters*

Fig. 7 depicts the variations in the oscillation frequency of the methane flame with the equivalence ratio. Each data point in Fig. 7 is the mean of 20 repeated measurements. The standard deviation of the 20 measurements is computed and given as an error bar in Fig. 7. Each measurement includes 2048 successive images. The trends of the data are fitted by the rational polynomials [43] and plotted in Fig. 7. As can be seen from Fig. 7, the oscillation frequency increases with the equivalence ratio, suggesting that the flame becomes more stable with an increasing equivalence ratio. This result is consistent with the conclusions from previous studies [44].

Table V summarises the correlation coefficient of the flame parameters with flame oscillation frequency. Each flame parameter in the table is the average of 20 measurements. In this study, the flame parameter is considered ‘effective’ if the correlation coefficient is above 0.8. This criterion is set due to the fact that the correlation coefficient is far below 0.80 if the variability contains little information about the flame stability. Thus, the height, area, area of root region, maximum temperature, minimum temperature, and mean temperature are effective, and the brightness as well as nonuniformity are ineffective.

Fig. 8 shows the variability of the eight flame parameters with equivalence ratio. For the effective parameters, the variability decrease with equivalence ratio. With a smaller equivalence ratio (less than 0.8), the significant variability suggest that the flame shape and temperature change substantially, and the root is not attached to the burner outlet stably. With a large equivalence ratio (larger than 1.2), the flame is stable, and the variability are small. The stable state of the flame is well characterised by these parameters. With regard to the ineffective parameters (i.e., brightness and

Table II. Biomass fuels and their blends tested and their compositions by weight

Fuel	Component
C50W50	50% Corncob + 50% Willow
C50P50	50% Corncob + 50% Peanut shell
C50S50	50% Corncob + 50% Wheat straw
W50P50	50% Willow + 50% Peanut shell
W50S50	50% Willow + 50% Wheat straw
P50S50	50% Peanut shell + 50% Wheat straw
P100	100% Peanut shell
W100	100% Willow
S100	100% Wheat straw
C100	100% Corncob

Table III. Proximate and ultimate analysis of the biomass fuels (as received)

Parameter	Peanut shell	Willow	Wheat straw	Corncob
Proximate Analysis (wt%)				
Moisture content	7.87	9.70	10.18	5.87
Volatile matter content	70.23	69.93	58.66	74.55
Ash content	4.21	3.22	17.58	1.34
Fixed carbon content	17.69	17.14	13.58	18.24
Ultimate analysis (wt%)				
C	43.03	44.67	32.17	39.68
O	49.52	49.24	63.18	59.62
H	5.56	5.33	3.97	<0.1
S	0.51	0.56	0.43	0.51
N	1.37	0.20	0.26	0.19

Table IV. Size and shape distributions of the biomass fuels.

Parameter	Peanut shell	Willow	Wheat straw	Corncob
Particle shape	Flake-like	cylindrical	Needle-like	Near-spherical
Aspect ratio (longest diameter/shortest diameter)	1.68 ± 0.75	3.28 ± 0.74	4.14 ± 1.76	1.45 ± 0.12
Particle size (μm) (min–max)	23.72 - 317.69	74.02 - 391.77	81.25 - 463.54	93.41 - 393.65
Mean particle size (μm)	171.27	213.27	243.97	230.78

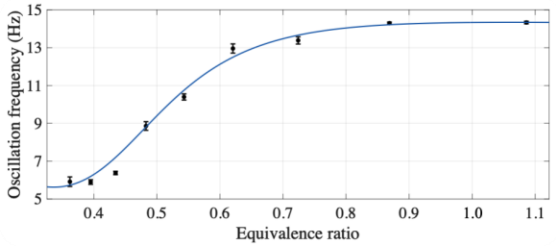

(a) 0.50 L/min methane flow rate

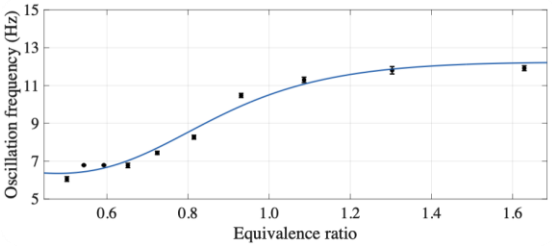

(b) 0.75 L/min methane flow rate

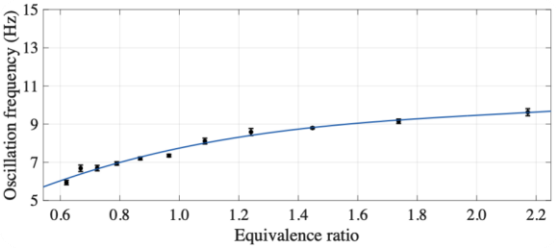

(c) 1.00 L/min methane flow rate

Fig. 7. Variation in oscillation frequency with equivalence ratios.

Table V Correlation coefficients between the oscillation frequency and the variability of flame parameters.

Methane flow rate (L/min)	L	A	A_{root}	B_f	NU_f	T_{max}	T_{min}	T_{mean}
0.50	0.96	0.96	0.95	0.71	0.69	0.94	0.98	0.97
0.75	0.88	0.90	0.81	0.73	0.66	0.95	0.85	0.84
1.00	0.91	0.90	0.83	0.32	0.40	0.95	0.91	0.91

nonuniformity), on the other hand, their variability increase first and then decrease with the equivalence ratio. This is attributed to the change in the flame colour from blue to yellow as the significant variability stems from the alternating colours.

Note that the height and area exhibit a similar variation with equivalence ratio due to the combustion characteristics of the laminar premixed flame. Since the flame area contains more spatial information than just the flame length, the variability of the length is not incorporated in evaluating the flame stability. Just like the area, since the mean temperature contains the thermal information from the maximum and minimum temperatures, only the variability of the mean temperature is incorporated in the flame stability evaluation.

2) *Instability coefficient of the effective parameters*

Fig. 9 exhibits the dependence of instability coefficients on the equivalence ratio for the area (A), area of the root region (A_{root}) and mean temperature of the flame (T_{mean}). It can be seen that the instability coefficients as well as corresponding standard deviations decrease with the equivalence ratio. This

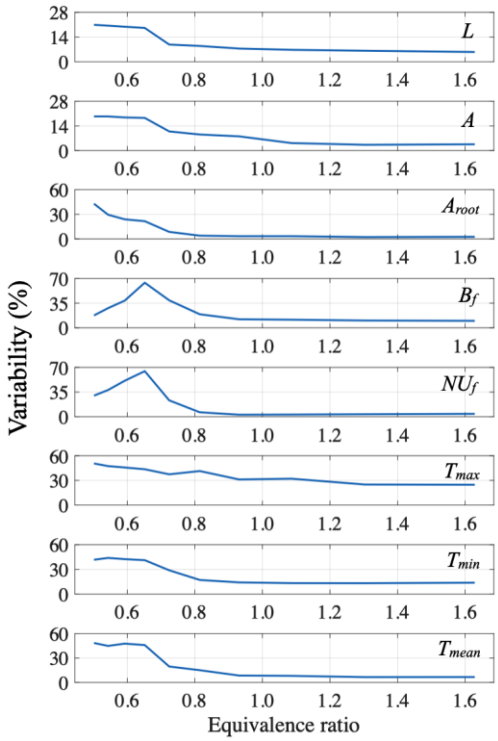

Fig. 8. Variability of each parameter with equivalence ratio for 0.75 L/min methane flow rate.

trend is attributed to the decreasing unusual values of the parameters as the flame becomes stable. These coefficients reflect the flame stability to a certain extent. Although the instability coefficients present a decreasing trend, it does not mean that the parameters become less sensitive to changes in the flame stability. Such a comparison is only conducted between the parameters under the same combustion conditions.

Figs. 8 and 9 demonstrates that the variability and instability coefficient of the mean temperature (T_{mean}) are mostly higher than those of the area (A) and area of the root region (A_{root}) across the range of equivalence ratios, indicating T_{mean} is the most important parameter. Figs. 8 and 9 also show that the variability and instability coefficient of the area of the root region increase rapidly near the lowest equivalent ratio. Since the methane flame cannot suspend stably above the outlet under the current combustion conditions, the irregular changes of the root lead to significant variability and hence large instability coefficients.

3) *Flame stability index for different equivalence ratios*

The stability index of methane flames with equivalence ratio, which is determined using the proposed method in comparison to the two reference methods (i.e., "multiplication" and "root-square" methods), are depicted in Figs. 10, 11, and 12. As shown in Figs. 10(a), 11(a) and 12(a), the proposed stability index decreases with the equivalence ratio, which is similar with the variation in the oscillation frequency. Their correlation coefficients are 0.96, 0.89, and 0.95 for methane flow rates of 0.50 L/min, 0.75 L/min, and 1.00 L/min, respectively. This result indicates that the proposed flame stability evaluation method performs well.

As illustrated in Figs. 10(b), 11(b) and 12(b), although the flame stability determined using the "multiplication" method

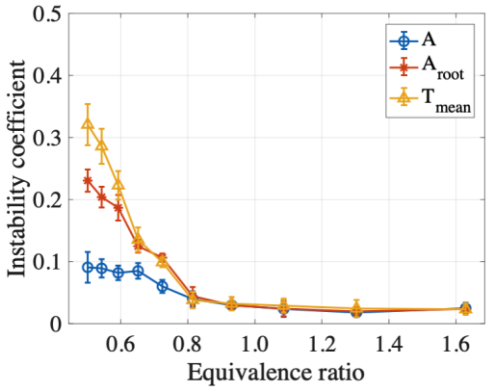

Fig. 9. Instability coefficients of the effective parameters for methane flow rates of 0.75 L/min.

decreases with the equivalence ratio, there are some local maxima and minima. These peaks should not appear due to the gradually increasing equivalence ratio, as shown in the flame stability results from the proposed method (Figs. 10(a), 11(a), and 12(a)). Apart from the local peaks, the standard deviations of the flame stability result from this reference method in the form of error bars, are significant with reference to the means, implying that incorrect flame stability evaluation could be made with insufficient measurements. As demonstrated in Figs. 10(c), 11(c) and 12(c) as well as Fig. 8, the flame stability result from the "root-square" method is heavily dependent upon the variability of the brightness and nonuniformity, whereas these two parameters are ineffective in the proposed method.

4) *Comparison between the oscillation frequency and stability index*

Figs. 10(a), 11(a) and 12(a) reveal that the variation trend of the flame stability index is consistent with that of the oscillation frequency. Such a trend is also reflected in the relatively high level of correlation coefficients (0.96, 0.89, and 0.95). However, the data length may affect this trend. Figs. 13 and 14 present the oscillation frequency and stability index as well as their standard deviations for different data lengths. The methane flow rate is 0.75 L/min. Each data point in Figs. 13(a) and 14(a) is the mean of 20 measurements. Note that in this case the standard deviation is normalised to the range of the mean, and the results are plotted on Figs. 13(b) and 14(b).

Fig. 13 illustrates that, as the data length is greater than 256, the oscillation frequency exhibits a similar trend and the normalised standard deviation falls a narrow range, suggesting that the flame stability is well characterised. However, it is evident in Fig. 14 that the stability index for the six data lengths has more or less the same trend. This consistent flame stability result is different from the oscillation frequency, regardless of the data length. Moreover, the normalised standard deviation of the stability index is much smaller than that of the oscillation frequency. This means the flame stability index is more reliable than the oscillation frequency. Besides, the stability index has more sensitive response to the variation in the flame stability. As the most stable flame changes to the most unstable one, the oscillation frequency decreases by about 50%, while the stability index increases by about 90%.

As mentioned above, the data length affects the determination of the oscillation frequency. Such an effect

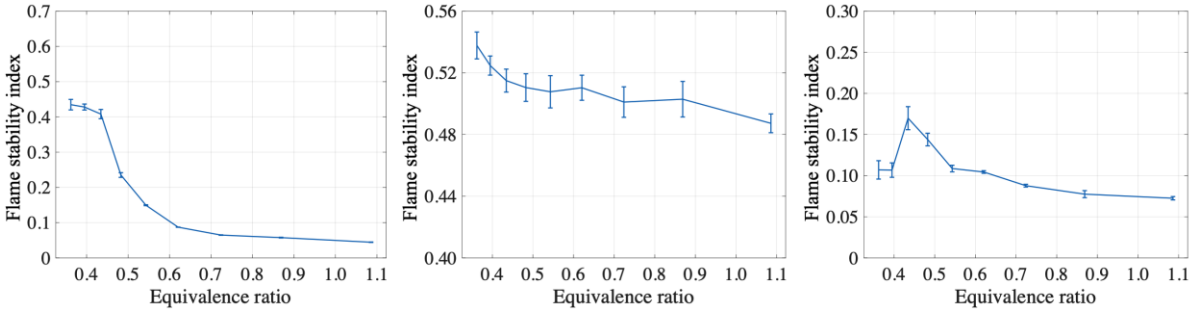

(a) The proposed method (b) Multiplication (c) Root-square

Fig. 10. Comparison of the flame stability results for methane flow rate 0.50 L/min.

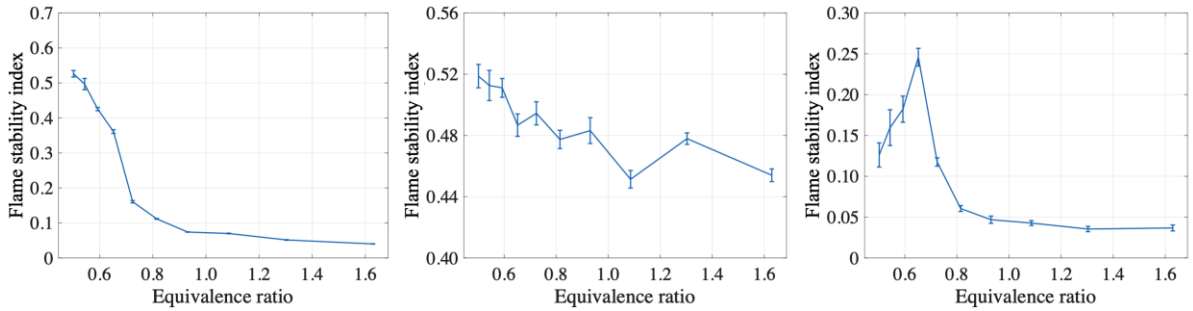

(a) The proposed method (b) Multiplication (c) Root-square

Fig. 11. Comparison of the flame stability results for methane flow rate 0.75 L/min.

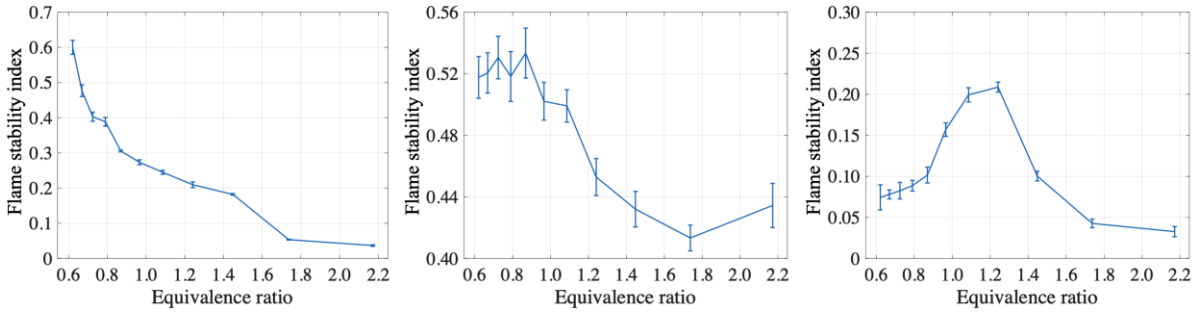

(a) The proposed method (b) Multiplication (c) Root-square

Fig. 12. Comparison of the flame stability results for methane flow rate 1.00 L/min.

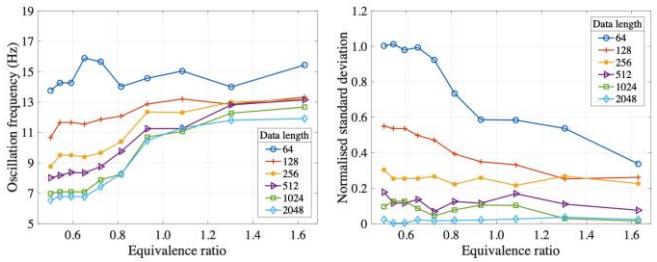

(a) Oscillation frequency (b) Normalised standard deviation

Fig. 13. Oscillation frequency for different data lengths.

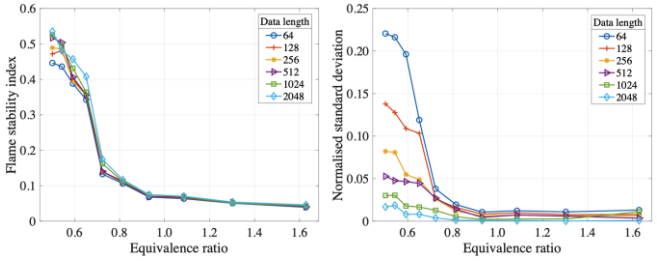

(a) Flame stability index (b) Normalised standard deviation

Fig. 14. Flame stability index for different data lengths.

originates from the increasing frequency resolution with a higher data length. As the data length is shorter, i.e. lower frequency resolution, the oscillation frequency spectrum is determined by a fewer number of frequency components. In this instance, the few frequency components as well as their constantly changing amplitudes lead to a higher standard deviation of the oscillation frequency. Additionally, unlike the diffusion methane flame which has a dominant peak on its power spectral density, a premixed flame has frequency components spread over low and high frequency parts with a range of amplitudes. With an increasing data length, the higher frequency resolution makes the high amplitudes in the low-frequency band have more significant influence on the determination of the weighted oscillation frequency than the low amplitudes in the high-frequency band, resulting in decreased oscillation frequency (Fig. 13(a)). When the data length is 512 or greater, due to the sufficient frequency resolution, the oscillation frequency does not change significantly with the data length and hence small standard deviation.

As displayed in Fig. 14, the stability index results are consistent for different data lengths.When the flame is unstable,

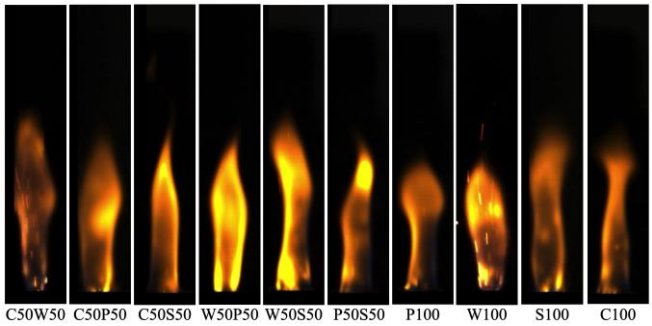

Fig. 15. Typical images of ten biomass flames.

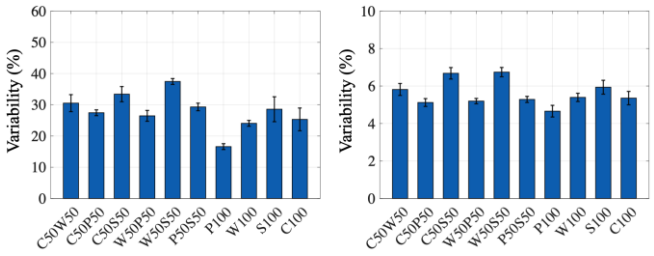

(a) Brightness (b) Mean temperature

Fig. 16. Variability of the brightness (B_f) and mean temperature (T_{mean}).

a short data length may not contain sufficient information to characterise the flame parameters. As a consequence, a subtle difference may occur in the resulting stability index between different data lengths, as denoted in Fig. 14(a). Nevertheless, even with a relatively small data length, the stability index is still consistently better than the oscillation frequency.

B. Biomass flames

1) *Effective flame parameters*

Fig. 15 depicts typical flame images of the ten biomass fuels. The biomass particles, pneumatically conveyed to the burner, combust at the flame root region and burn out at the flame tip region, as can be seen in Fig. 15 (C50W50). The oscillation frequency of each biomass flame and variability of each flame parameter are obtained with 1024 successive images. Table VI summarises the correlation coefficients of the flame parameters. It is clear that the variability of the brightness and mean temperature correlate well with the oscillation frequency. These two parameters are considered effective and thus incorporated in the flame stability evaluation. The reason for these two effective parameters is that their variability are closely related to the particle size. Since chemicals in the fuel particles do not vary with their sizes, the combustion of smaller particles yields similar levels of brightness and temperature and hence the flames are of small variability in these two parameters [45]. As summarised in Table IV, the peanut shell has the smallest range (23.72-317.69 μm), and thus the peanut shell flame has the smallest variability in the brightness and mean temperature, as plotted in Fig. 16. By the same token, the wheat straw has the widest particle size range (81.25 - 463.54 μm), and thus the wheat straw flame has the most significant variability in the brightness and mean temperature (Fig. 16).

On the contrary and as summarised in Table VI, the length, area, area of the root region, nonuniformity, maximum and minimum temperatures of the flames are considered to be 'ineffective'. The length and area are strongly related to the

Table VI. Correlation coefficients between the oscillation frequency and the variability of flame parameters.

Parameter	L	A	A_{root}	B_f	NU_f	T_{max}	T_{min}	T_{mean}
Correlation coefficient	0.39	0.03	0.14	0.85	0.26	0.21	0.42	0.88

aerodynamics of the flame. However, the differences in the flames of the ten biomass fuels are insignificant and thus their flame stability is not reflected in the variability of the length and area. Since all the flames are attached to the burner outlet stably, the variability of the area of the root region does not contain much flame stability information. The reason for the ineffective nonuniformity, maximum and minimum temperatures is similar. The nonuniformity is determined by the difference between the light and dark regions, which should link to the maximum and minimum temperatures, respectively. The light and dark regions are believed to be due to a small number of particles the sizes of which are relatively small and large, respectively. These particles do not affect the flame stability significantly due to the relatively small proportions, but do lead to variability in the nonuniformity, maximum and minimum temperatures.

2) *Flame stability*

Fig. 17 plots the oscillation frequency and stability index for the flame of 10 biomass fuels. It is clear that the oscillation frequency and stability index are consistent to each other, and their correlation coefficient is 0.91, indicating that the stability index represents well the stability of the biomass flames. The stability index (Fig.17(b)) is superior to the oscillation frequency in two folds. First, it is evident that the stability index has smaller standard deviation than the oscillation frequency, which is plotted as error bars in Fig.17, demonstrating more reliable approach to flame stability assessment. Second, Fig. 17(a) as well as Figs. 7(a) and 10(a) show that the oscillation frequency decreases by about 20% while the stability index increases by about 50% as the biomass fuel addition to the methane flame, manifesting deteriorating flame stability. The change in the stability index of the biomass fuels is obviously more significant, indicating a more sensitive response to flame stability.

Fig. 17(b) shows that the stability of the wheat straw flame is the worst amongst the four pure biomass fuels. This can be explained by the fact that wheat straw is the least combustible fuel in terms of chemical composition and particle shape (Tables 3 and 4). In contrast, the peanut shell flame is most stable due primarily to the fineness and small aspect ratio of the particles of this fuel (Table IV).

The flame stability of the biomass blends is poorer than that of the four pure biomass fuels. Further research is required to study this phenomenon from a combustion science perspective. Fig. 17(b) also shows that the flames of the three corncob blends, i.e., with peanut shell (C50P50), willow (C50W50) and wheat straw (C50S50) blends are the most, second, and worst stable, respectively. This outcome is consistent with the comparison between the flame stability results for the three individual biomass fuels. This means a blended fuel flame is more stable if the blend contains a fuel with better flame stability.

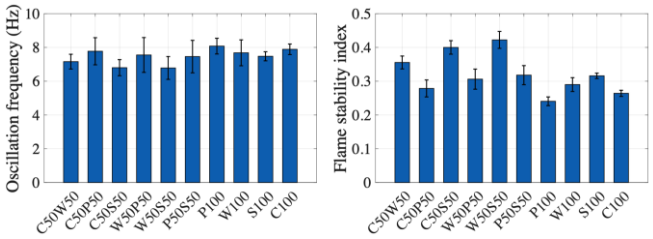

(a) Oscillation frequency (b) Flame stability index

Fig. 17. Flame stability represented in terms of oscillation frequency and flame stability index for biomass fuels.

V. Conclusion

A novel method for quantitatively assessing burner flame stability through digital imaging and image processing has been proposed. Results obtained have demonstrated that, for the premixed methane flame over the range of equivalence ratios 0.36 to 2.17 and biomass flames, the proposed method characterises the flame stability. The correlation coefficients between the proposed flame index and the oscillation frequency are greater than 0.89. Experimental results have suggested that a better flame stability result is achieved with the proposed method than the two reference methods, i.e. "multiplication" and "root-square" methods. Experimental results have also demonstrated that, over the range of data lengths 64 to 2048, the discrepancy in the results from the oscillation frequency is significant whereas the stability index results are consistent, indicating that the calculation for a reliable stability index requires less data than the oscillation frequency.

The results have shown that the stability index yields a more sensitive response than the oscillation frequency to changes in flame stability. When the premixed methane flame changes from the most stable state (large equivalence ratio) to the most unstable one (small equivalence ratios), its oscillation frequency decreases by about 50%, while its stability index increases by about 90%. Meanwhile, the oscillation frequency of the biomass flames decreases by about 20% whilst the stability index increases by about 50%. The flame stability index has been utilized to quantify the stability of biomass fuels and their blends. It is found that the flame stability of the blended biomass fuels is consistently poorer than that of the individual pure biomass fuels. Moreover, a blended biomass flame is stabler if the blend contains a fuel with better flame stability.

References

[1] A. A. Bhuiyan, A. S. Blicblau, AKMS Islam and J. Nasera, "A review on thermo-chemical characteristics of coal/biomass co-firing in industrial furnace," *Journal of the Energy Institute*, vol. 91, no. 1, pp. 1-18, 2018.

[2] R. Zhang, F. Hao and W. Fan, "Combustion and stability characteristics of ultra-compact combustor using cavity for gas turbines," *Applied Energy*, vol. 225, 1 September 2018, pp. 940–954.

[3] C. Zhou, Y. Wang, Q. Jin, Q. Chen and Y. Zhou, "Mechanism analysis on the pulverized coal combustion flame stability and NOx emission in a swirl burner with deep air staging," *Journal of the Energy Institute*, vol. 92, no. 2, pp. 298–310, 2019.

[4] T. Chi, H. Zhang, Y. Yan, H. Zhou and H. Zheng, "Investigations into the ignition behaviors of pulverized coals and coal blends in a drop tube furnace using flame monitoring techniques," *Fuel*, vol. 89, no. 3, pp. 743–751, 2010.

[5] H.J. Burbano, J. Pareja and A.A. Amell, "Laminar burning velocities and flame stability analysis of H2/CO/air mixtures with dilution of N2 and CO2," *International Journal of Hydrogen Energy*, vol. 36, no. 4, pp. 3232–3242, 2011.

[6] M. Bauerheim, F. Nicoud and T. Poinsot, "Theoretical analysis of the mass balance equation through a flame at zero and non-zero Mach numbers," *Combustion and Flame*, vol. 162, no. 1, pp. 60-67, 2015.

[7] Z.X.Chen, I. Langella, N. Swaminathan, M. Stöhrb, W. Meierb and H. Kollac, "Large Eddy Simulation of a dual swirl gas turbine combustor: Flame/flow structures and stabilisation under thermoacoustically stable and unstable conditions," *Combustion and Flame*, vol. 203, pp. 279-300, 2019.

[8] R. Honza, C.P. Ding, A. Dreizler and B. Böhm, "Flame imaging using planar laser induced fluorescence of sulfur dioxide," *Applied Physics B*, vol. 123, Art. no. 246, 2017.

[9] L.H. Ma, L.Y. Lau and W. Ren, "Non-uniform temperature and species concentration measurements in a laminar flame using multi-band infrared absorption spectroscopy,". *Applied Physics B*, vol. 123, Art. no. 83, 2017.

[10] D. Sun, G. Lu, H. Zhou, Y. Yan and S. Liu, "Quantitative Assessment of Flame Stability Through Image Processing and Spectral Analysis," *IEEE Transactions on Instrumentation and Measurement*, vol. 64, no. 12, pp. 3323-3333, 2015.

[11] J. Ballester, T and García-Armingol, "Diagnostic techniques for the monitoring and control of practical flames," *Progress in Energy and Combustion Science*, vol. 36, no. 4, pp. 375-411, 2010.

[12] M.G. De Giorgi, A. Sciolti, S. Campilongo and A. Ficarella. "Image processing for the characterization of flame stability in a non-premixed liquid fuel burner near lean blowout," *Aerospace Science and Technology*, vol. 49, pp. 41-51, 2016.

[13] J. Pan, J.A. Libera, N.H. Paulson and M. Stan, "Flame Stability Analysis of Flame Spray Pyrolysis by Artificial Intelligence," *The International Journal of Advanced Manufacturing Technology*, vol. 114, pp. 2215–2228, 2021.

[14] Y. Huang, Y. Yan, G. Lu and A. Reed, "On-line flicker measurement of gaseous flames by image processing and spectral analysis," *Measurement Science and Technology*, vol. 10, pp. 726-733, 1999.

[15] J. Matthes, P. Waibel, M. Vogelbacher, H.J. Gehrmann and H.B. Keller, "A new camera-based method for measuring the flame stability of non-oscillating and oscillating combustions," *Experimental Thermal and Fluid Science*, vol. 105, pp. 27-34, 2019.

[16] M. Chimenti, C. Di Natali, G. Mariotti, E. Paganini, G. Pieri and O. Salvetti, "An IR image processing approach for characterizing combustion instability," *Infrared Physics & Technology*, vol. 46, no. 1, pp.41-47, 2004.

[17] G. Lu, Y. Yan, S. Cornwell, M. Whitehouse and G. Riley, "Impact of co-firing coal and biomass on flame characteristics and stability," *Fuel*, vol. 87, pp. 1133-1140, 2008.

[18] D. Durox, T. Yuan and E. Villermaux, "The effect of buoyancy on flickering in diffusion flames," *Combustion Science and Technology*, vol. 124, no. 1, pp. 277-294, 1997.

[19] K.B. Sahu, A. Kundu, R. Ganguly and A. Datta, "Effects of fuel type and equivalence ratios on the flickering of triple flames," *Combustion and Flame*, vol. 156, no. 2, pp. 484-493, 2009.

[20] H.G. Darabkhani and Y. Zhang, "Methane diffusion flame dynamics at elevated pressures," *Combustion Science and Technology*, vol. 182, no. 3, pp. 231-251, 2010.

[21] K.R.V. Manikantachari, V. Raghavan and K. Srinivasan, "Effects of burner configurations on the natural oscillation characteristics of laminar jet diffusion flames," *International Journal of Spray and Combustion Dynamics*, vol. 7, no. 3, pp. 257-281, 2015.

[22] J. Smart, G. Lu, Y. Yan and G. Riley, "Characterisation of an oxy-coal flame through digital imaging," *Combustion and Flame*, vol. 157, no. 6, pp. 1132-1139, 2010.

[23] B.B. Samantaray and C.K. Mohanta, "Analysis of industrial flame characteristics and constancy study using image processing technique," *Journal of Mechanical Engineering and Sciences*, vol. 9, pp. 1604-1613, 2015.

[24] M. Najarnikoo, M.Z. Targhi and H. Pasdarshahri, "Experimental study on the flame stability and color characterization of cylindrical premixed perforated burner of condensing boiler by image processing method," *Energy*, vol. 189, Art. no. 116130, 2019.

[25] D. Sun, G. Lu, H. Zhou, X. Li and Y. Yan, "A simple index based quantitative assessment of flame stability," *IEEE International Conference on Imaging Systems and Techniques*, pp. 190-193, 2013.

[26] D. Sun, G. Lu and Y. Yan, "An embedded imaging and signal processing system for flame stability monitoring and characterization," *IEEE*

International Conference on Imaging Systems and Techniques, pp. 210-213, 2010.

[27] G. Lu, Y. Yan and M. Colechin, "A digital imaging based multifunctional flame monitoring system," *IEEE Transactions on Instrumentation and Measurement*, vol. 53, no. 4, pp. 1152-1158, 2004.

[28] G. Lu, Y. Yan, M. Colechin and R. Hill, "Monitoring of oscillatory characteristics of pulverized coal flames through image processing and spectral analysis," *IEEE Transactions on Instrumentation and Measurement*, vol. 55, no. 1, pp. 226-231, 2006.

[29] S. Choi, T.Y. Kim, H.K. Kim, J. Koo, J.S. Kim and O.C. Kwon, "Properties of inverse nonpremixed pure O2/CH4 coflow flames in a model combustor," *Energy*, vol. 93, pp. 1105-1115, 2015.

[30] H.M. Altay, S. Park, D. Wu, D. Wee, A.M. Annaswamy and A.F. Ghoniem, "Modeling the dynamic response of a laminar perforated-plate stabilized flame," *Proceedings of the Combustion Institute*, vol. 32, no. 1, pp. 1359-1366, 2009.

[31] J.C. Massey, Z.X. Chen and N. Swaminathan, "Lean flame root dynamics in a gas turbine model combustor," *Combustion Science and Technology*, vol. 191, no. 5, pp. 1019-1042, 2019.

[32] F. Shum-Kivan, J. Marrero Santiago, A. Verdier, E. Riber, B. Renou, G. Cabot and B. Cuenot, "Experimental and numerical analysis of a turbulent spray flame structure," *Proceedings of the Combustion Institute*, vol. 36, no. 2, pp. 2567-2575, 2017.

[33] P.M. Allison, K. Frederickson, J.W. Kirik, R.D. Rockwell, W.R. Lempert and J.A. Suttona, "Investigation of supersonic combustion dynamics via 50 kHz CH* chemiluminescence imaging," *Proceedings of the Combustion Institute*, vol. 36, no. 2, pp. 2849-2856, 2017.

[34] Y.M. Al-Abdeli and A.R. Masri, "Turbulent swirling natural gas flames: Stability characteristics, unsteady behavior and vortex breakdown," *Combustion Science and Technology*, vol. 179, no. 1, pp. 207-225, 2007.

[35] C. Saravanan, "Color Image to Grayscale Image Conversion," *2010 Second International Conference on Computer Engineering and Applications*, pp. 196-199, 2010.

[36] T. Seidel, G. Krishnamoorthy and W.S. Seames, "Characterizing flame stability and radiative heat transfer in non-swirling oxy-coal flames using different multiphase modeling frameworks," *Fuel*, vol. 256, Art. no. 115948, 2019.

[37] D. Sun, G. Lu, H. Zhou and Y. Yan, "Flame stability monitoring and characterization through digital imaging and spectral analysis," *Measurement Science and Technology*, vol. 22, Art. no. 114007, 2011.

[38] G. Lu, Y. Yan, G. Riley and H.C. Bheemul, "Concurrent measurement of temperature and soot concentration of pulverized coal flames," *IEEE Transactions on Instrumentation and Measurement*, vol. 51, no. 5, pp. 990-995, 2002.

[39] H. Uchiyama, M. Nakajima and S. Yuta, "Measurement of flame temperature distribution by IR emission computed tomography," *Applied Optics*, vol. 24, no. 23, pp. 4111-4116, 1985.

[40] B. Nie, X. He, C. Zhang, X. Li and H. Li, "Temperature measurement of gas explosion flame based on the radiation thermometry," *International Journal of Thermal Sciences*, vol. 78, pp. 132-144, 2014.

[41] J. O'Connor and T. Lieuwen, "Further characterization of the disturbance field in a transversely excited swirl-stabilized flame," *Journal of Engineering for Gas Turbines and Power*, vol. 134, no. 1, Art. no. 011501, 2012.

[42] P. Stavropoulos, A. Michalakou, G. Skevis and S. Couris, "Laser-induced breakdown spectroscopy as an analytical tool for equivalence ratio measurement in methane–air premixed flames," *Spectrochimica Acta Part B: Atomic Spectroscopy*, vol. 60, no. 7, 31 August 2005, pp. 1092-1097.

[43] E.S. Bañuelos-Cabral, J.A. Gutierrez-Robles and B. Gustavsen, "Rational fitting techniques for the modeling of electric power components and systems using MATLAB environment," *IntechOpen*, 2017.

[44] D. Fritsche, M. Füri and K. Boulouchos, "An experimental investigation of thermoacoustic instabilities in a premixed swirl-stabilized flame," *Combustion and Flame*, vol. 151. no. 1, pp. 29-36, 2007.

[45] Y.B. Yang, V. N. Sharifi, J. Swithenbank, L. Ma, L.I. Darvell, J.M., Jones, M. Pourkashanian and A. Williams, "Combustion of a single particle of biomass," *Energy & Fuels*, vol. 22, no. 1, pp. 306-316, 2008.